HOKKAIDO UNIVERSITY

Title	Encapsulant-Dependent Effects of Long-Term Low-Temperature Annealing on Interstitial Defects in Mg-Ion-Implanted GaN
Author(s)	Akazawa, Masamichi; Murai, Shunta; Kachi, Tetsu
Citation	Journal of electronic materials, 51(4), 1731-1739 https://doi.org/10.1007/s11664-022-09431-y
Issue Date	2022-02-03
Doc URL	http://hdl.handle.net/2115/87883
Rights	This version of the article has been accepted for publication, after peer review (when applicable) and is subject to Springer Nature's AM terms of use, but is not the Version of Record and does not reflect post-acceptance improvements, or any corrections. The Version of Record is available online at: http://dx.doi.org/10.1007/s11664-022-09431-y
Type	article (author version)
File Information	JEM51_Akazawa_final ver.pdf

Encapsulant-Dependent Effects of Long-Term Low-Temperature Annealing on Interstitial Defects in Mg-Ion-Implanted GaN

Masamichi AKAZAWA[1,3], Shunta MURAI[1], and Tetsu KACHI[2]

[1]*Research Center for Integrated Quantum Electronics, Hokkaido University, Sapporo, Hokkaido 060-0813, Japan*

[2]*Institute of Materials and Systems for Sustainability, Nagoya University, Nagoya, Aichi 464-8601, Japan*

[3]e-mail: akazawa@rciqe.hokudai.ac.jp

The encapsulant-dependent effects of long-term low-temperature annealing on defects in Mg-ion-implanted GaN have been investigated using metal-oxide-semiconductor (MOS) diodes. Annealing was carried out at 600 °C under nitrogen flow without or with a cap layer of Al_2O_3, SiO_2, or SiN. For annealing at 600 °C for 3 h, the capacitance–voltage characteristics of the Al_2O_3 cap annealed samples indicated the existence of acceptor-like defects, whereas those of the capless, SiO_2 cap and SiN cap annealed samples exhibited bumps, which indicated the existence of donor-like defect level at around 0.8 eV from the conduction band edge E_C. A more distinct result was obtained for annealing at 600 °C for 30 h. Namely, annealing of samples with the Al_2O_3 cap layer induced an acceptor-like defect level at $E_C - 0.9$ eV, whereas that with the SiN cap layer induced a donor-like defect level at $E_C - 0.8$ eV. Secondary ion mass spectroscopy and transmission electron microscopy studies revealed that interstitial Ga (Ga_i) in Mg-implanted GaN diffused into the Al_2O_3 cap layer but not into the SiN cap layer after annealing. Most possibly, the detected $E_C - 0.8$ eV level can be assigned to interstitial Ga_i.

Key words: GaN, Mg ion implantation, annealing, MOS, defect levels, encapsulant

INTRODUCTION

GaN is a promising material for achieving high-efficiency high-power electronic devices [1–3] because of its wide band gap [3], high breakdown field [4], high electron mobility [3], and high saturation electron velocity [5]. Compared with other widegap semiconductors, a notable advantage of this material is availability of constructing heterostructures with various nitride alloys, *i.e.*, AlGaN, InAlN, InGaN, and InAlGaN, which expands the flexibility of the device design [6–9]. Furthermore, insulator/GaN interfaces can be controlled to minimize interface states [10–13], which enables us to realize power metal-oxide-semiconductor (MOS) field-effect transistors (FETs) using GaN as a channel material. In the fabrication of power devices, ion implantation is a convenient method for selective doping. For GaN, however, ion implantation for forming p-type doping regions is challenging. Although Mg ion implantation is considered the most promising way, it has been generally difficult to obtain a high activation ratio. Recently, however, successful formation of p-type regions in GaN by Mg ion implantation has been reported [14–22]. In particular, ultra-high-pressure annealing (UHPA) of Mg-ion-implanted GaN under 1 GPa nitrogen at 1400 °C has been reported to realize a high activation ratio through the reduction of N-vacancy (V_N)-related defects [22]. This technique is a breakthrough for Mg-ion implantation of GaN. On the other hand, however, developing an activation annealing method in a conventional furnace using atmospheric-pressure nitrogen flow is also important. For this purpose, a low-temperature annealing method for controlling defects generated by Mg ion implantation should be established, which requires a study on defect levels in Mg-ion-implanted GaN.

The control of defects in Mg-ion-implanted GaN may be possible by annealing at a temperature much lower than that necessary for Mg activation. The effects of low-temperature annealing on defects in Mg-ion-implanted GaN have been studied in detail by deep-level transient spectroscopy (DLTS) using Schottky barrier diodes [23] and capacitance–voltage (C–V) methods using MOS diodes [24–28]. On the basis of a DLTS study, several defect levels at 0.2 – 1.0 eV from the conduction band edge E_C were detected and found to vary depending on the annealing temperature up to 1000 °C [23]. Moreover, the C–V method for the MOS diodes revealed an acceptor-like defect level located at 0.7 – 0.8 eV from E_C for Mg implantation at 50 keV and a dose of 1.5×10^{11} cm^{-2} and that located at 0.2 – 0.3 eV from E_C at a higher Mg dose of 1.5×10^{12} cm^{-2} [24–27]. The origin of the former level is likely to be interstitial N (N$_i$) [26], whereas that of the latter level was found to be the divacancies of Ga and N ($V_{Ga}V_N$), as determined by the combination of the C–V

2

method and positron annihilation spectroscopy (PAS) [28]. However, it was also found that $V_{Ga}V_N$ was the dominant vacancy defect under the as-implanted condition and even after low-temperature annealing, independent of dose [28, 29]. Nevertheless, a sample with an Al_2O_3 cap layer with annealing at 600 °C for 3 min was found to show improved $C–V$ characteristics of the MOS diode with Mg-ion-implanted GaN at a Mg dose of 1.5×10^{11} cm^{-3} compared with a sample without 600 °C annealing [25]. Furthermore, an extension of the annealing duration led to further improvement of the $C–V$ characteristics of the MOS diode with the same structure. Namely, annealing of a sample with the Al_2O_3 cap layer at 600 °C for 3 h further improved the $C–V$ characteristics [26]. Since $V_{Ga}V_N$ was reported to persist for annealing at a temperature as high as 1000 °C [29], the behavior of N_i seems to be related to the observed improvement of the $C–V$ characteristics.

Vacancy defects might be eliminated by combining them with interstitial defects. However, there has been no report on the control of interstitial defects in Mg-ion-implanted GaN to the best of our knowledge. In particular, when V_{Ga} is occupied by interstitial Mg (Mg_i) to form Mg in a Ga site (Mg_{Ga}), interstitial Ga (Ga_i) should remain. Therefore, the control of Ga_i and N_i seems to be important for realizing high performance of completed p-type GaN. To realize this goal, we should understand the behavior of these interstitial defects upon low-temperature annealing.

There is possibility that defects in Mg-ion-implanted GaN may be affected by the encapsulant or cap layer material used for a sample during annealing. If it is possible to control the density of target defects in Mg-ion-implanted GaN by low-temperature cap annealing prior to high-temperature annealing, a method for the highly efficient activation of implanted Mg atoms may be developed. For example, pulling out Ga_i by its diffusion from Mg-ion-implanted GaN into a cap layer during low-temperature annealing may promote coupling between Mg_i and V_{Ga} to form Mg_{Ga} instead of coupling between Ga_i and V_{Ga}. Therefore, it is worthwhile to study the effects of the cap layer material used during low-temperature annealing on the electrical characteristics of Mg-ion-implanted GaN.

We report here that the encapsulant material during long-term low-temperature annealing affects the behavior of interstitial defects in Mg-ion implanted GaN. MOS diodes used for the investigation of the near-surface region in GaN were fabricated and tested after long-term low-temperature annealing of Mg-ion-implanted GaN using various encapsulants. Basically, many types of point defect can exist in Mg-implanted GaN. However, if defects of one type diffuse toward the GaN surface upon annealing and reach a high density at the surface, the resultant defect distribution considerably affects the electrical characteristics of

the MOS diodes. Therefore, we can detect a deep level originating from defects with high diffusivity, which may lead to the determination of the encapsulant-dependent difference in the behavior of the defects upon annealing.

EXPERIMENTAL METHODS

The sample fabrication sequence is shown in Fig. 1. A 3-μm-thick Si-doped Wurtzite GaN epitaxial layer with a carrier concentration of 5×10^{17} cm^{-3} was grown by metalorganic vapor phase epitaxy (MOVPE) on a free-standing n^+-GaN (0001) substrate via an n^+-GaN buffer layer. Mg ions were implanted at room temperature at an energy of 50 keV and a dose of 1.5×10^{11} cm^{-2}. The resultant depth profiles of Mg and Si concentrations, [Mg] and [Si], respectively, analyzed by secondary ion mass spectroscopy (SIMS) are shown in Fig. 2. It can be seen that [Mg] is well below [Si]. Therefore, we can expect that the n-type conduction in GaN remain in the implanted samples. For SIMS and transmission electron microscopy (TEM) measurements, a sample with a high Mg dose of 1.5×10^{12} cm^{-2} was also prepared. After the Mg ion implantation, low-temperature annealing was carried out at 600 °C for 3 h or 30 h under nitrogen flow without or with a cap layer of Al_2O_3, SiO_2, or SiN. Al_2O_3 was formed by atomic layer deposition (ALD) at 300 °C using trimethylaluminum and H_2O, whereas SiO_2 and SiN were deposited by RF sputtering at room temperature. After annealing, the cap layers were removed with a solution of HF:H_2O = 1:1. Subsequently, a new Al_2O_3 insulating layer of 30 nm thickness prepared by ALD, Ni/Au top electrodes, and a Ti/Au back ohmic contact were formed to complete a MOS diode. Finally, postmetallization annealing (PMA) was carried out at 300 °C for 3 h in air to minimize the interface state density [6, 7]. A MOS structure enables the study of the near-surface region, which is difficult for Schottky barrier diodes. Therefore, in this work, electrical properties of the Mg-ion-implanted GaN were studied by C–V measurement of the fabricated MOS diodes.

RESULTS AND DISCUSSION

The C–V characteristics of the samples annealed at 600 °C for 3 h are summarized in Fig. 3 for various encapsulants used during annealing. Here, the flat band voltage of the ideal curve was adjusted to coincide with that of the C–V curves of a control sample, *i.e.*, an *n*-GaN MOS diode fabricated without Mg ion implantation or 600 °C annealing. An anomalously steep region of the C–V curves of the Al_2O_3 cap annealed sample appeared on the positive bias side of the ideal curve, as shown in Fig. 3(a). This indicates that an acceptor-like defect level was dominant in the GaN bulk. However, the C–V curves of all other samples exhibited

bumps, as shown in Figs. 3(b)–(d), which may have been caused by electron traps localized in the vicinity of the GaN surface. All bumps were seen only in the C–V curves with the *capture* bias sweep from the negative voltage to the positive voltage. This was because the capture of an electron by an electron trap was much faster than the emission of an electron as follows, where the time constant τ_E for the electron emission from an electron trap at energy E_T is given by [23, 30–32]

$$\tau_E = \frac{1}{\sigma v_{th} N_C} exp\left(\frac{E_C - E_T}{kT}\right), \tag{1}$$

where σ is the capture cross section of the electron trap, v_{th} is the thermal velocity of electrons, N_C is the effective density of states in E_C, k is the Boltzmann constant, and T is the temperature. On the other hand, the electron capture time constant τ_C is given by [30, 33, 34]

$$\tau_C = \frac{1}{\sigma v_{th} n}, \tag{2}$$

where n is the volume density of carrier electrons. Under band bending, n at the surface becomes smaller than that in the bulk because of carrier depletion. Since the carrier concentration n_S at the GaN surface is expressed as a function of the surface Fermi level E_{FS} as

$$n_S = N_C exp\left(-\frac{E_C - E_{FS}}{kT}\right), \tag{3}$$

the electron capture time constant τ_{CS} at the GaN surface is given by

$$\tau_{CS} = \frac{1}{\sigma v_{th} N_C} exp\left(\frac{E_C - E_{FS}}{kT}\right). \tag{4}$$

This is the maximum value of τ_C for the electron traps in the vicinity of the surface. At the topmost surface, $\tau_C = \tau_{CS}$. However, even at a shallow point inside the bulk, $\tau_C < \tau_{CS}$. The calculation results of τ_E or τ_{CS} are plotted as a function of $E_C - E_T$ or $E_C - E_{FS}$, respectively, in Fig. 4 for various σ values. In the C–V measurement, the bias voltage was changed in steps of 50 mV at 1 s intervals. As shown by the calculation results in Fig. 4, τ_E becomes much larger than 1 s when $E_C - E_T$ is larger than 0.7 eV. In this case, a C–V curve for the *emission* bias sweep from the positive voltage to the negative voltage does not show a bump because

the electron emission does not follow the bias sweep. Although τ_E is constant independent of E_{FS}, τ_{CS} varies exponentially depending on E_{FS}. Therefore, the measured $C–V$ curves with a bump for the *capture* bias sweep may indicate the existence of a defect level deeper than 0.7 eV. Moreover, bumps appeared on the negative bias side of the ideal curves shown in Figs. 3(b)–(d), which indicated that the charge of the defect level localized in the vicinity of the GaN surface was positive when unoccupied and neutral when occupied. Therefore, the dominant defect level was the donor-like level for the capless, SiO_2 cap and SiN cap annealed samples.

The electron trap density D_T distribution was derived from the measured 1 MHz $C–V$ curve for each sample, using the high-frequency method [35]. The derived D_T distributions for samples annealed for 3 h are shown in Fig. 5 for the samples (a) with a SiO_2 cap layer, (b) without a cap layer, and (c) with a SiN cap layer. Note that no D_T distribution for the 3-h-Al_2O_3-cap-annealed sample was detected because the measured $C–V$ curve was steeper than the ideal one at the shallow depletion region. This might be due to the acceptor-like defect levels related to $V_{Ga}V_N$ [28] and N_i. Discrete levels corresponding to the bumps in the $C–V$ curves can be seen at $0.7 – 0.8$ eV from the conduction band edge E_C. According to the disorder-induced gap state model [36, 37], which is a guiding principle for interface states, the interface state distribution at the insulator–semiconductor interface should be U-shaped over the entire band gap. Actually, U-shaped interface state distributions have been reported for GaN MOS structures [38, 39]. However, when specific high-density bulk defects exist near the interface, a discrete defect level can be observed [40, 41]. Therefore, the detected discrete levels in Figs. 5(a), (b), and (c) likely originated from the bulk defects in the vicinity of the GaN surface. In Fig. 3, the encapsulant-dependent magnitude order of the hysteresis due to the bumps is SiN cap layer > no cap layer > SiO_2 cap layer among the samples with the donor-like defect level. Actually, the density of defect levels was in the same order among these samples.

As shown in Fig. 3, the SiN cap annealed sample showed the largest bump in the $C–V$ curves, whereas the Al_2O_3 cap annealed sample showed no distinct bump despite the opposite shift of the $C–V$ curves. For the Al_2O_3 cap annealed sample, the extension of the annealing duration from 3 min to 3 h at 600 °C slightly improved the $C–V$ characteristics; thus, we extended the duration further, expecting a further improvement. However, the obtained result was unexpected. By applying longer-term annealing for 30 h to these extremes, we obtained the $C–V$ characteristics shown in Fig. 6(a) for the sample with the Al_2O_3 cap layer and Fig. 6(b) for the sample with the SiN cap layer. Bumps appeared in the

C–V curves for the *capture*, or negative-to-positive, bias sweep even for the Al_2O_3 cap annealed sample. A distinct difference dependent on the encapsulant can be seen between these samples, *i.e.*, the bumps in the *C–V* curves appeared on the opposite sides of the ideal curve. The bump in the *C–V* curves of the Al_2O_3-cap-layer sample appeared on the positive bias side of the ideal curve, indicating that the defect level is an acceptor-like state. However, the bump in the *C–V* curves of the sample with the SiN cap layer appeared on the negative bias side of the ideal curve, indicating that the defect level is a donor-like state.

To estimate the energy of the defect level, D_T distributions were derived from the measured 1 MHz *C–V* curves of the 30-h annealed samples. The results are shown in Fig. 7. It can be seen that D_T distributions of both samples contained discrete levels. The locations of the detected discrete level in the band gap were $E_C - 0.9$ eV and $E_C - 0.8$ eV for the Al_2O_3-cap-layer sample and the SiN-cap-layer sample, respectively. As described above, these discrete levels are considered the defect levels in the GaN bulk. Considering the behavior of the *C–V* curves, the $E_C - 0.9$ eV level detected for the Al_2O_3-cap-layer sample should have been an acceptor-like level, whereas the $E_C - 0.8$ eV level detected for the SiN-cap-layer sample should have been a donor-like level. According to previous reports [42–44], the acceptor-like level at $E_C - 0.9$ eV and the donor-like level at $E_C - 0.8$ eV might be assigned to N_i and Ga_i, respectively.

The difference between the observed defect levels likely resulted from the diffusion of defects. The diffusion coefficient D is given by

$$D = D_0 exp\left(-\frac{E_A}{kT}\right), \tag{5}$$

where D_0 is the frequency factor and E_A is the activation energy. Although E_A is generally given by the sum of the migration barrier E_M and formation energy of defects, it is equal to E_M in Mg-ion-implanted GaN, where a nonequilibrium density of defects exists, as discussed in our previous report [28]. According to a previous report [45], the magnitude order of E_M of simple defects in *n*-GaN tended to be $V_N > V_{Ga} > N_i > Ga_i$. Therefore, the migration of Ga_i and N_i may have played a key role. Although the parameters of diffusion of defects from GaN into Al_2O_3, SiO_2, and SiN layers have not yet been reported, there is a possibility that Ga_i diffused into the Al_2O_3 cap layer during long-term 600 °C annealing with N_i remaining in GaN, whereas the diffusion of Ga_i was blocked by the SiN cap layer, resulting in the pile up of Ga_i at the interface.

To investigate the diffusion of Ga atoms, SIMS was carried out. Figure 8(a) shows the

Ga concentration [Ga] profile measured by SIMS for SiN (~20 nm)/low-dose-Mg-implanted GaN structure after 600 °C annealing for 30 h in comparison with that for the control sample of SiN/GaN without implantation or annealing. It can be seen that both profiles overlap each other, which shows that Ga diffusion is below the detection limit of 10^{17} cm^{-3}. However, for the samples with an Al$_2$O$_3$ cap layer, a completely different result was obtained. In Fig. 8(b), SIMS [Ga] profiles for Al$_2$O$_3$ (~20 nm)/low-dose (1.5×10^{11} cm^{-2})-Mg-implanted GaN and Al$_2$O$_3$/high-dose (1.5×10^{12} cm^{-2})-Mg-implanted GaN structures after 600 °C annealing for 30 h are plotted in comparison with that for the control sample of Al$_2$O$_3$/GaN without implantation or annealing. The trace of the Ga diffusion can be seen for the Mg-implanted samples. Note that the higher Mg ion dose led to a higher [Ga] in Al$_2$O$_3$. This result indicated that the extent of the Ga diffusion was increased depending on the Mg ion dose. Therefore, the diffused Ga atoms are related to the Mg ion implantation.

The possibility that the Ga diffusion into Al$_2$O$_3$ was caused by the intermixing between Al$_2$O$_3$ and Mg-implanted GaN was denied as follows. Figure 9 shows a cross-sectional TEM image of the Al$_2$O$_3$/high-dose Mg-implanted GaN sample after 600 °C annealing for 30 h. Around the Al$_2$O$_3$/GaN interface, no intermixing was indicated. Furthermore, a SIMS result (not shown here) for the implanted GaN after annealing of the same condition showed no evidence of Al diffusion into GaN from the Al$_2$O$_3$ layer. Therefore, the Ga diffusion observed in Fig. 8(b) was not caused by intermixing, indicating that it is highly likely that the Ga$_i$ generated by Mg ion implantation diffused into the Al$_2$O$_3$ layer, whereas SiN blocked the Ga$_i$ diffusion. We can safely conclude that the detected donor-like deep level at $E_C - 0.8$ eV for the SiN-cap, SiO$_2$-cap, and capless annealing can be assigned to Ga$_i$.

An analysis of the micro strain in the implanted GaN to investigate the effects of long-term low-temperature annealing is an interesting issue. X-ray diffraction (XRD) is a powerful tool to analyze the micro strain [46–50]. Actually, XRD analysis of ion-implanted GaN has been reported [51, 52]. However, the Mg ion implantation for the present samples was carried out with an extremely low dose and a shallow depth. Therefore, it is difficult to analyze the strain precisely according to the previous report [52]. Samples implanted with higher dose and higher energy should be prepared and analyzed, which is the future work.

SUMMARY

The encapsulant-dependent effects of long-term 600 °C annealing on Mg-ion-implanted GaN was investigated using MOS diodes. For 600 °C/3 h annealing, the C–V characteristics of the Al$_2$O$_3$ cap annealed sample indicated the existence of acceptor-like defects, whereas

those of the capless, SiO$_2$ cap and SiN cap annealed samples exhibited a bump, which indicated the existence of donor-like defects. For the samples except the Al$_2$O$_3$ cap layer sample, a defect level at around 0.8 eV below E_C was detected. A more distinct result was obtained for 600 °C/30 h annealing. Namely, annealing with the Al$_2$O$_3$ cap layer induced an acceptor-like defect level at E_C – 0.9 eV, whereas that with the SiN cap layer induced a donor-like defect level at E_C – 0.8 eV. The evidence of the diffusion of Ga$_i$ generated in GaN by Mg ion implantation into the Al$_2$O$_3$ cap layer was obtained by SIMS and TEM, whereas the SiN cap layer blocked the Ga$_i$ diffusion into it. Therefore, the donor-like defect level at E_C – 0.8 eV can be assigned to Ga$_i$. Moreover, the detected acceptor-like defect level at E_C – 0.9 eV might be assigned to N$_i$ according to the calculated energy level and the tendency of the migration barrier magnitude among the point defects in previous reports [38, 41].

ACKNOWLEDGMENTS

CONFLICT OF INTEREST

On behalf of all authors, the corresponding author states that there is no conflict of interest.

References

[1]   T. Kachi, Recent progress of GaN power devices for automotive applications. Jpn. J. Appl. Phys. 53, 100210 (2014).

[2]   H. Amano, Y Baines, E. Beam, M. Borga, T. Bouchet, P. R Chalker, M. Charles, K. J. Chen, N. Chowdhury, R. Chu, C. De Santi, M. M. De Souza, S. Decoutere, L. Di Cioccio, B. Eckardt, T. Egawa, P. Fay, J. J. Freedsman, L. Guido, O. Häberlen, G. Haynes, T. Heckel, D.   Hemakumara, P. Houston, J. Hu, M. Hua, Q. Huang, A. Huang, S. Jiang, H Kawai, D. Kinzer, M. Kuball, A. Kumar, K. B. Lee, X. Li, D. Marcon, M. März, R. McCarthy, G. Meneghesso, M. Meneghini, E. Morvan, A. Nakajima, E. M. S. Narayanan, S. Oliver, T. Palacios, D. Piedra, M. Plissonnier, R. Reddy, M. Sun, I. Thayne, A. Torres, N. Trivellin, V. Unni, M. J. Uren, M. V. Hove, D. J. Wallis, J. Wang, J. Xie, S. Yagi, S. Yang, C. Youtsey, R. Yu, E. Zanoni, S. Zeltner, Yuhao Zhang, The 2018 GaN power electronics roadmap. J. Phys. D, Appl. Phys. 51, 163001 (2018).

[3]   D. Ueda, in Power GaN Devices, ed. by M. Meneghini, G. Meneghesso, and E. Zanoni, (Springer, New York, 2017), p. 1.

[4]   B.J. Baliga, Gallium nitride devices for power electronic applications. Semicond. Sci. Technol. 28, 074011 (2013).

[5]   F. Schwierz, An electron mobility model for wurtzite GaN. Solid-State Electronics 49, 889 (2005).

[6]   P.A. Alvi, S. Gupta, M. J. Siddiqui, G. Sharma, S. Dalela, Modeling and simulation of GaN/Al$_{0.3}$Ga$_{0.7}$N new multilayer nano-heterostructure. Physica B 405, 2431 (2010).

[7]   P.A. Alvi, S. Gupta, P. Vijay, G. Sharma, M.J. Siddiqui, Affects of Al concentration on GaN/Al$_x$Ga$_{1-x}$N newmodeled multilayer nano-heterostructure. Physica B 405, 3624 (2010).

[8]   S. Gupta, F. Rahman, M.J. Siddiqui, P.A. Alvi, Strain profile in nitride based multilayer nano-heterostructures, Physica B 411, 40 (2013).

[9]   S. Ahmad, M.A. Raushan, S. Kumar, S. Dalela, M.J. Siddiqui, P.A. Alvi, Modeling and simulation of GaN based QW LED for UV emission, Optik 158, 1334 (2018).

[10] S. Kaneki, J. Ohira, S. Toiya, Z. Yatabe, J. T. Asubar, T. Hashizume, Highly-stable and low-state-density Al$_2$O$_3$/GaN interfaces using epitaxial n-GaN layers grown on free-standing GaN substrates. Appl. Phys. Lett. 109, 162104 (2016).

[11] T. Hashizume, S. Kaneki, T. Oyobiki, Y. Ando, S. Sasaki, K. Nishiguchi, Effects of postmetallization annealing on interface properties of Al$_2$O$_3$/GaN structures. Appl. Phys. Express 11, 124102 (2018).

[12] T. Yamada, J. Ito, R. Asahara, K. Watanabe, M. Nozaki, T. Hosoi, T. Shimura, H. Watanabe, Improved interface properties of GaN-based metal-oxide-semiconductor devices with thin Ga-oxide interlayers. Appl. Phys. Lett. 110, 261603 (2017).

[13] T. Yamada, D. Terashima, M. Nozaki, H. Yamada, T. Takahashi, M. Shimizu, A. Yoshigoe, T. Hosoi, T. Shimura, H. Watanabe, Controlled oxide interlayer for improving reliability of SiO$_2$/GaN MOS devices. Jpn, J. Appl. Phys. 58, SCCD06 (2019).

[14] B. N. Feigelson, T. J. Anderson, M. Abraham, J. A. Freitas, J. K. Hite, C. R. Eddy, F. J. Kub, Multicycle rapid thermal annealing technique and its application for the electrical activation of Mg implanted in GaN. J. Cryst. Growth 350, 21 (2012).

[15] T. J. Anderson, B. N. Feigelson, F. J. Kub, M. J. Tadjer, K. D. Hobart, M. A. Mastro, J. K. Hite, C. R. Eddy, Activation of Mg implanted in GaN by multicycle rapid thermal annealing. Electron. Lett. 50, 197 (2014).

[16] J. D. Greenlee, T. J. Anderson, B. N. Feigelson, K. D. Hobart, F. J. Kub, Characterization of an Mg-implanted GaN p–i–n diode. Phys. Status Solidi A 212, 2772 (2015).

[17] T. J. Anderson, J. D. Greenlee, B. N. Feigelson, J. K. Hite, K. D. Hobart, F. J. Kub, Improvements in the Annealing of Mg Ion Implanted GaN and Related Devices. IEEE Trans. Semicond. Manuf. 29, 343 (2016).

[18] K. Nomoto, K. Takahashi, T. Oikawa, H. Ogawa, T. Nishimura, T. Mishima, H. G. Xing, T. Nakamura, Ion Implantation into GaN and Implanted GaN Power Transistors. ECS Trans. 69, 105 (2015).

[19] T. Oikawa, Y. Saijo, S. Kato, T. Mishima, T. Nakamura, Formation of definite GaN p–n junction by Mg-ion implantation to n⁻-GaN epitaxial layers grown on a high-quality free-standing GaN substrate. Nuclear Instruments and Methods in Physics Research B 365, 168 (2015).

[20] T. Niwa, T. Fujii, T. Oka, High carrier activation of Mg ion-implanted GaN by conventional rapid thermal annealing. Appl. Phys. Express 10, 091002 (2017).

[21] T. Narita, T. Kachi, K. Kataoka, T. Uesugi, Electric-field-induced simultaneous diffusion of Mg and H in Mg-doped GaN prepared using ultra-high-pressure annealing. Appl. Phys. Exp. 10, 016501 (2017).

[22] H. Sakurai, M. Omori, S. Yamada, Y. Furukawa, H. Suzuki, T. Narita, K. Kataoka, M. Horita, M. Bockowski, J. Suda, T. Kachi, Highly effective activation of Mg-implanted p-type GaN by ultra-high-pressure annealing. Appl. Phys. Lett. 115, 142104 (2019).

[23] G. Alfieri, V.K. Sundaramoorthy, R. Micheletto, Electrically active point defects in Mg implanted n-type GaN grown by metal-organic chemical vapor deposition. J. Appl. Phys. 123, 205303 (2018).

[24] M. Akazawa, N. Yokota, K. Uetake, Detection of deep-level defects and reduced carrier concentration in Mg-ionimplanted GaN before high-temperature annealing. AIP Advances 8, 025310 (2018).

[25] M. Akazawa, K. Uetake, Impact of low-temperature annealing on defect levels generated by Mg-ion-implanted GaN. Jpn. J. Appl. Phys. 58, SCCB10 (2019).

[26] M. Akazawa, R. Kamoshida, S. Murai, T. Narita, M. Omori, J. Suda, T. Kachi, Effects of Dosage Increase on Electrical Properties of Metal-Oxide-Semiconductor Diodes with Mg-Ion-Implanted GaN Before Activation Annealing. Phys. Status Solidi B 257, 1900367 (2020).

[27] M. Akazawa, R. Kamoshida, Analysis of simultaneous occurrence of shallow surface Fermi level pinning and deep depletion in MOS diode with Mg-ion-implanted GaN before activation annealing. Jpn. J. Appl. Phys. 59, 096502 (2020).

[28] M. Akazawa, R. Kamoshida, S. Murai, T. Kachi, A. Uedono, Low-temperature annealing behavior of defects in Mg-ion-implanted GaN studied using MOS diodes and monoenergetic positron beam. Jpn. J. Appl. Phys. 60, 016502 (2021).

[29] A. Uedono, S. Takashima, M. Edo, K. Ueno, H. Matsuyama, W. Egger, T. Koschine, C. Hugenschmidt, M. Dickmann, K. Kojima, S.F. Chichibu, S. Ishibashi, Carrier Trapping by Vacancy-Type Defects in Mg-Implanted GaN Studied Using Monoenergetic Positron Beams. Phys. Status Solidi B 255, 1700521 (2018).

[30] W. Shockley, W. T. Read, Statistics of the recombinations of holes and electrons. Phys. Rev. 87, 835 (1952).

[31] P. Hacke, T. Detchprohm, K. Hiramatsu, N. Sawaki, K. Tadatomo, K. Miyake, Analysis of deep levels in n-type GaN by transient capacitance methods. J. Appl. Phys. 76, 304 (1994).

[32] G. Brammertz, K. Martens, S. Sioncke, A. Delabie, M. Caymax, M. Meuris, M. Heyns, Characteristic trapping lifetime and capacitance-voltage measurements of GaAs metal-oxide-semiconductor structures. Appl. Phys. Lett. 91, 133510 (2007).

[33] F. Schmidt, H. Wenckstern, O. Breitenstein, R. Pickenhain, M. Grundmann, Low rate deep level transient spectroscopy - a powerful tool for defect characterization in wide bandgap semiconductors. Solid State Electron. 92, 40 (2014).

[34] J. Pavelka, J. Šikula, M. Tacano, M. Toita, Activation energy of RTS noise.

Radioengineering 20, 194 (2011).

[35] S. M. Sze, K. K. Ng, Physics of Semiconductor Devices, 3rd edn. (Wiley, Hoboken, NJ, 2007).

[36] H. Hasegawa, H. Ohno, Unified disorder induced gap state model for insulator-semiconductor and metal-semiconductor interfaces. J. Vac. Sci. & Technol. B 4, 1130 (1986).

[37] H. Hasegawa, M. Akazawa, Interface models and processing technologies for surface passivation and interface control in III–V semiconductor nanoelectronics. Appl. Surf. Sci 254, 8005 (2008).

[38] C. Mizue, Y. Hori, M. Miczec, T. Hashizume, Capacitance–Voltage Characteristics of Al_2O_3/AlGaN/GaN Structures and State Density Distribution at Al_2O_3/AlGaN Interface. Jpn. J. Appl. Phys. 50, 021001 (2011).

[39] M. Matys, B. Adamowicz, A. Domanowska, A. Michalewicz, R. Stoklas, M. Akazawa, Z. Yatabe, T. Hashizume, On the origin of interface states at oxide/III-nitride heterojunction interfaces. J. Appl. Phys. 120, 225305 (2016).

[40] T. Sawada, K. Numata, S. Tohdoh, T. Saitoh, H. Hasegawa, In-situ characterization of compound semiconductor surfaces by novel photoluminescence surface state spectroscopy. Jpn. J. Appl. Phys. 32, 511 (1993).

[41] T. Hashizume, R. Nakasaki, Discrete surface state related to nitrogen vacancy defect on plasma-treated GaN surfaces. Appl. Phys. Lett. 80, 4564 (2002).

[42] J. L. Lyons, C. G. Van de Walle, Computationally predicted energies and properties of defects in GaN. npj Comput. Mater. 3, 12 (2017).

[43] Z.-Q. Fang, D. C. Look, J. Jasinski, M. Benamara, Z. Liliental-Weber, R. J. Molnar, Evolution of deep centers in GaN grown by hydride vapor phase epitaxy. Appl. Phys. Lett. 78, 332 (2001).

[44] A. Y. Polyakov, N. B. Smirnov, A. V. Govorkov, A. V. Markov, N. G. Kolin, D. I. Merkurisov, V. M. Boiko, K. D. Shcherbatchev, V. T. Bublik, M. I. Voronova, I-H. Lee, C. R. Lee, S. J. Pearton, A. Dabirian, A. V. Osinsky, Fermi level pinning in heavily neutronirradiated GaN. J. Appl. Phys. 100, 093715 (2006).

[45] S. Limpijumnong, C. G. Van de Walle, Diffusivity of native defects in GaN. Phys. Rev. B 69, 035207 (2004).

[46] K.K. Khichar, S.B. Dangi, V. Dhayal, U. Kumar, S.Z. Hashmi, V. Sadhu, B.L. Choudhary, S. Kumar, S. Kaya, A.E. Kuznetsov, S. Dalela, S.K. Gupta, P.A.Alvi, Structural, optical, and surface morphological studies of ethyl cellulose/graphene

oxide nanocomposites. Polym. Compos. 41, 2792 (2020).

[47] B.L. Choudhary, U. Kumar, S. Kumar, S. Chander, S. Kumar, S. Dalela, S.N. Dolia, and P.A. Alvi, Irreversible magnetic behavior with temperature variation of $Ni_{0.5}Co_{0.5}Fe_2O_4$ nanoparticles. J. Magn. Magn. Mater. 507, 166861 (2020).

[48] V. Dhayal, S.Z. Hashmi, U. Kumar, B.L. Choudhary, A.E. Kuznetsov, S. Dalela, S. Kumar, S. Kaya, S.N. Dolia, P.A. Alvi, Spectroscopic studies, molecular structure optimization and investigation of structural and electrical properties of novel and biodegradable Chitosan-GO polymer nanocomposites. J. Mater. Sci. 55, 14829 (2020).

[49] G. Lal, K. Punia, S.N. Dolia, P.A. Alvi, B.L. Choudhary, S. Kumar, Structural, cation distribution, optical and magnetic properties of quaternary $Co_{0.4+x}Zn_{0.6-x}Fe_2O_4$ (x = 0.0, 0.1 and 0.2) and Li doped quinary $Co_{0.4+x}Zn_{0.5-x}Li_{0.1}Fe_2O_4$ (x = 0.0, 0.05 and 0.1) nanoferrites. J. Alloys Compd. 828, 154388 (2020).

[50] U. Kumar, S. Upadhyay, P.A. Alvi, Study of reaction mechanism, structural, optical and oxygen vacancy-controlled luminescence properties of Eu-modified Sr_2SnO_4 Ruddlesden popper oxide. Physica B: Phys. Condens. Matter. 604, 412708 (2021).

[51] B.J. Pong, C.J. Pan, Y.C. Teng, G.C. Chi, W.-H. Li, K.C. Lee, C.H. Lee, Structural defects and microstrain in GaN induced by Mg ion implantation. J. Appl. Phys. 83, 5992 (1998).

[52] P. Mendes, K. Lorenz, E. Alves, S. Schwaiger, F. Scholz, S. Magalhães, Measuring strain caused by ion implantation in GaN. Mater. Sci. Semicond. Process. 98, 95 (2019).
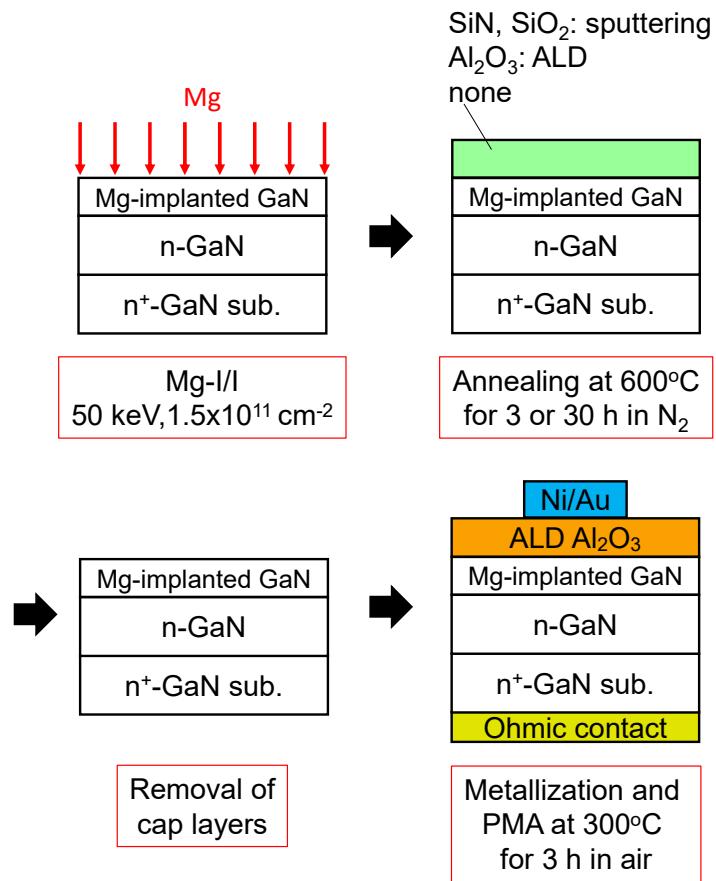
Figure captions

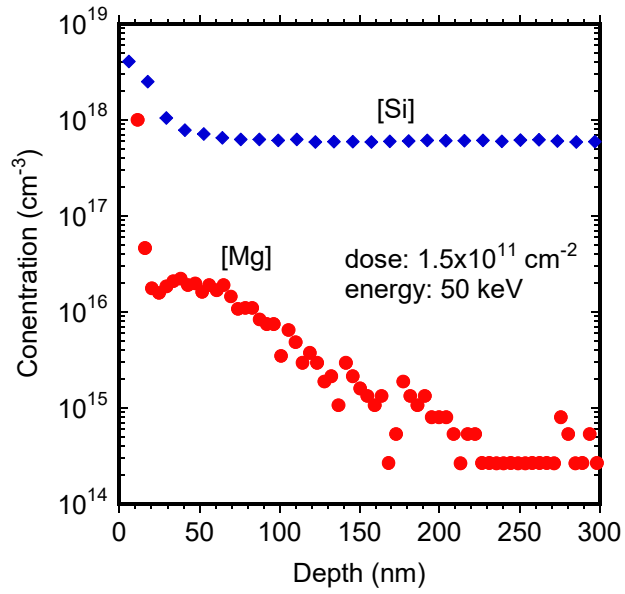**Fig. 1.** Sample fabrication sequence.

Fig. 2. SIMS [Mg] and [Si] profiles for as-implanted GaN. The [Mg] profile data is taken from our previous report [28] with permission (Copyright (2020) The Japan Society of Applied Physics).
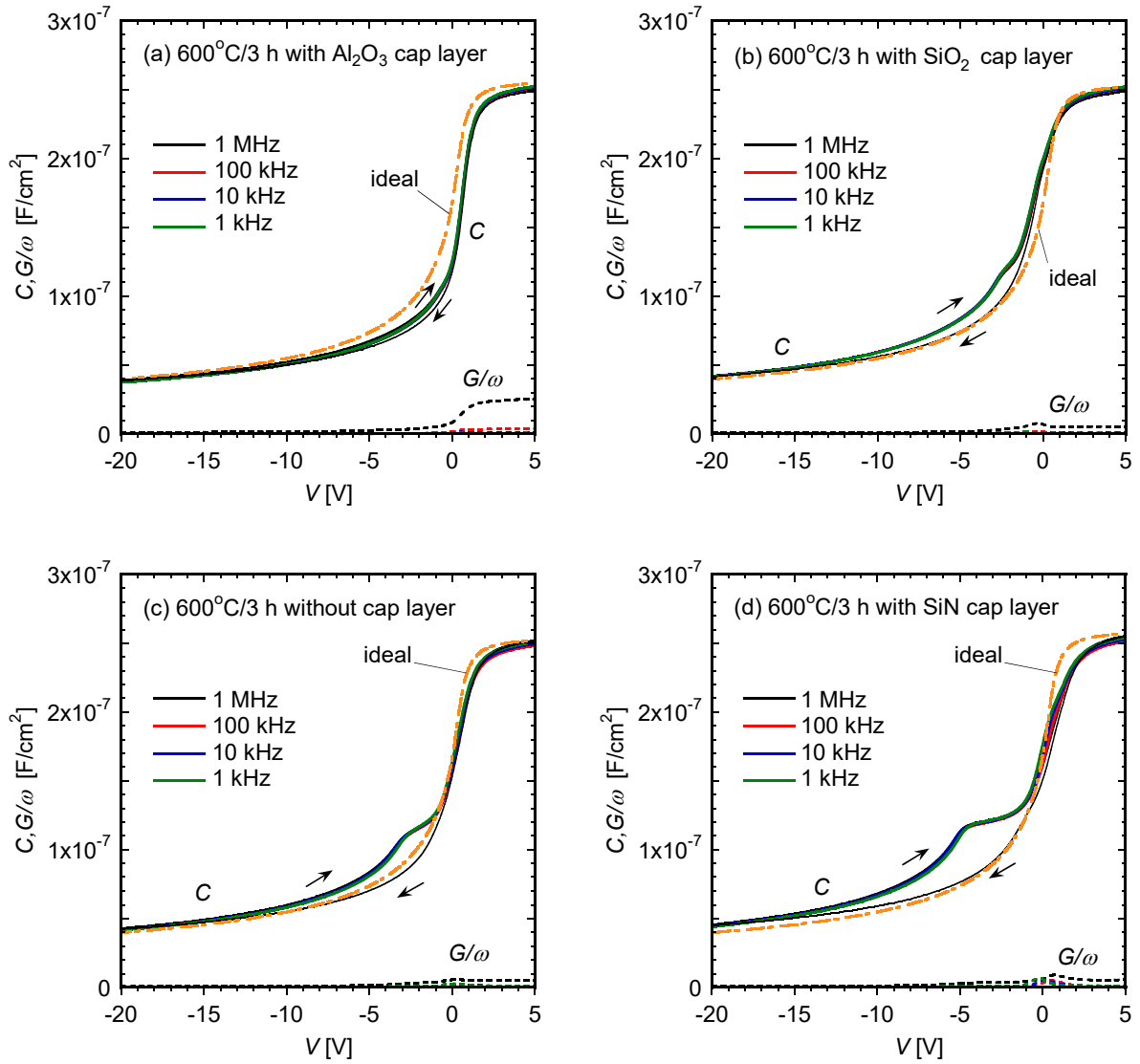
Fig. 3. C–V characteristics of samples annealed at 600 °C for 3 h with (a) Al_2O_3 cap layer, (b) SiO_2 cap layer, (c) no cap layer, and (d) SiN cap layer. To avoid complexity, only 1 MHz curves are plotted for the emission direction. Measured data in (a) is taken from our previous report [26] with permission (Copyright (2019) John Wiley& Sons).
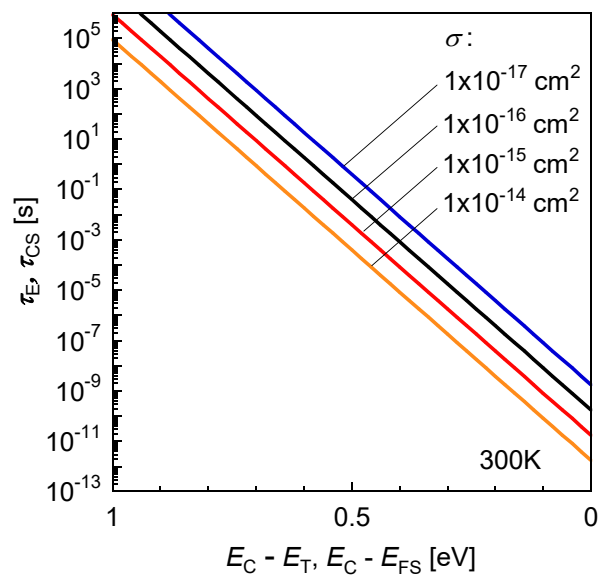
Fig. 4. τ_E and τ_{CS} calculated as functions of $E_C - E_T$ and $E_C - E_{FS}$, respectively, at various σ.
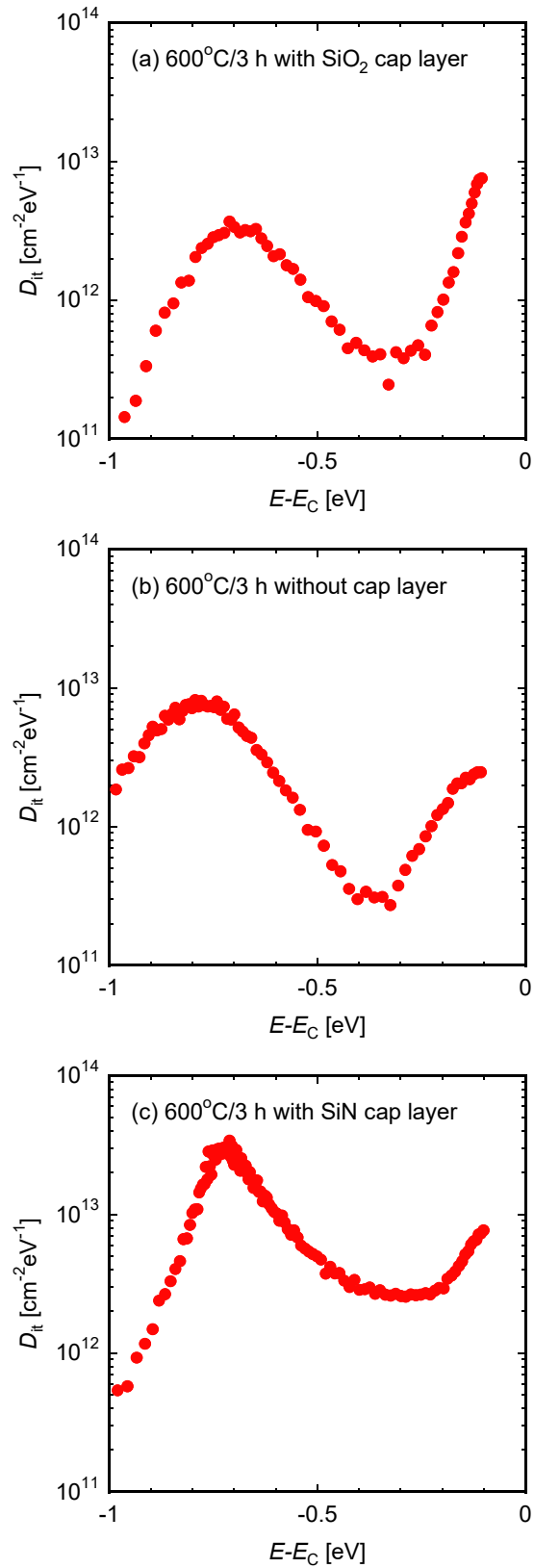
Fig. 5. D_T distribution for samples annealed at 600 °C for 3h with (a) SiO_2 cap layer, (b) no cap layer, and (c) SiN cap layer.

Fig. 6. C–V characteristics for samples annealed at 600 °C for 30 h with (a) Al_2O_3 cap layer and (b) SiN cap layer. To avoid complexity, only 1 MHz curves are plotted for the emission direction.

Fig. 7. D_T distribution for samples annealed at 600 °C for 30 h.

Fig. 8. [Ga] profiles measured by SIMS. (a) SiN/GaN samples. (b) Al_2O_3/GaN samples: samples implanted with Mg at dose of 1.5×10^{12} cm^{-2} (high dose) and 1.5×10^{11} cm^{-2} (low dose). Control samples are as-deposited samples.

Fig. 9. Near-interface cross-sectional TEM image of Al_2O_3/high-dose Mg-implanted GaN annealed at 600 °C for 30 h.

Fig. 1. Sample fabrication sequence.

Fig. 2. SIMS [Mg] and [Si] profiles for as-implanted GaN. The [Mg] profile data is taken from our previous report [28] with permission (Copyright (2020) The Japan Society of Applied Physics).

Fig. 3. *C–V* characteristics of samples annealed at 600 °C for 3 h with (a) Al_2O_3 cap layer, (b) SiO_2 cap layer, (c) no cap layer, and (d) SiN cap layer. To avoid complexity, only 1 MHz curves are plotted for the emission direction. Measured data in (a) is taken from our previous report [26] with permission (Copyright (2019) John Wiley& Sons).

Fig. 4. τ_E and τ_{CS} calculated as functions of $E_C - E_T$ and $E_C - E_{FS}$, respectively, at various σ.

Fig. 5. D_T distribution for samples annealed at 600 °C for 3h with (a) SiO$_2$ cap layer, (b) no cap layer, and (c) SiN cap layer.

Fig. 6. *C–V* characteristics for samples annealed at 600 °C for 30 h with (a) Al₂O₃ cap layer and (b) SiN cap layer. To avoid complexity, only 1 MHz curves are plotted for the emission direction.
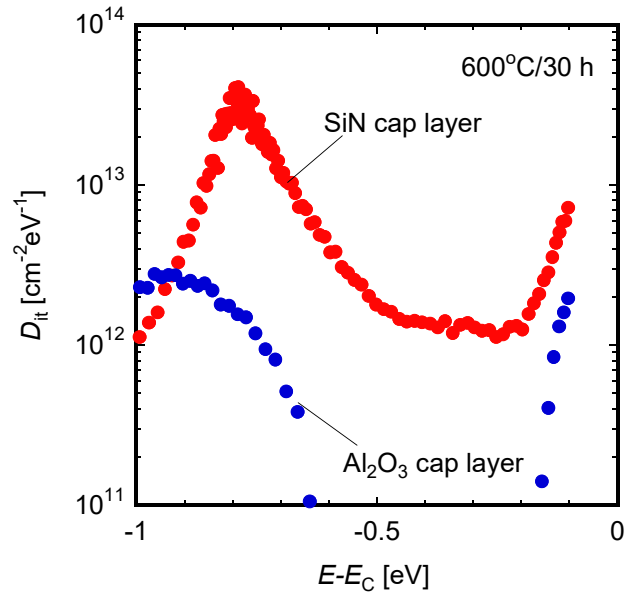
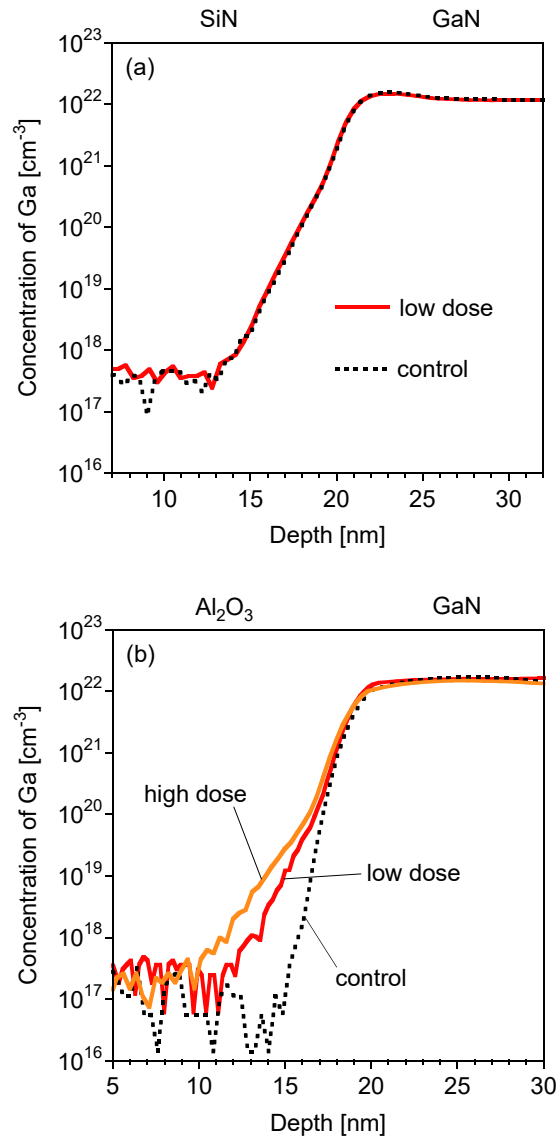**Fig. 7.** D_T distribution for samples annealed at 600 °C for 30 h.

Fig. 8. [Ga] profiles measured by SIMS. (a) SiN/GaN samples. (b) Al_2O_3/GaN samples: samples implanted with Mg at dose of 1.5×10^{12} cm^{-2} (high dose) and 1.5×10^{11} cm^{-2} (low dose). Control samples are as-deposited samples.
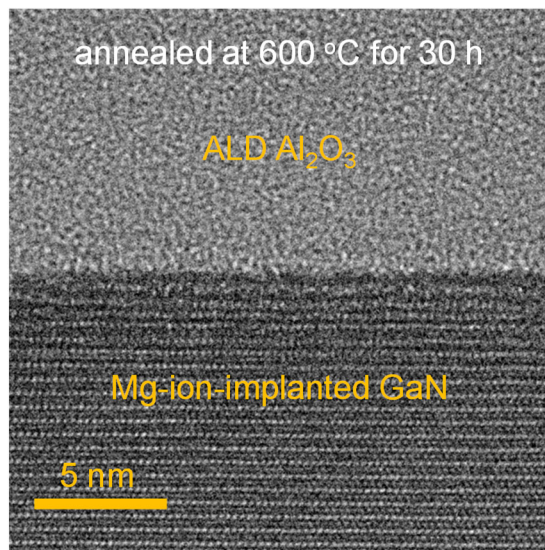
Fig. 9. Near-interface cross-sectional TEM image of Al_2O_3/high-dose Mg-implanted GaN annealed at 600 °C for 30 h.